Few-Body Systems 25, 115–132 (1998)

Few-Body Systems

Deuteron Electrodisintegration at High Missing Momenta*

W.-J. Kasdorp[1], W. H. A. Hesselink[1,2], D. Groep[1], E. Jans[1], N. Kalantar-Nayestanaki[3], L. Lapikás[1], J. J. van Leeuwe[1], A. Misiejuk[4], G. J. L. Nooren[1], C. J. G. Onderwater[1,2], A. R. Pellegrino[1,2], C. M. Spaltro[1,2], R. Starink[1,2], G. van der Steenhoven[1], J. J. M. Steijger[1], and J. A. Templon[1,2]

[1] Nationaal Instituut voor Kernfysica en Hoge-Energiefysica (NIKHEF), P.O. Box 41882, NL-1009 DB Amsterdam, The Netherlands
[2] Faculty of Physics and Astronomy, Vrije Universiteit, De Boelelaan 1081, NL-1081 HV Amsterdam, The Netherlands
[3] Kernfysisch Versnellerinstituut (KVI), Rijksuniversiteit Groningen, Zernikelaan 25, NL-9747 AA Groningen, The Netherlands
[4] Universiteit Utrecht, P.O. Box 80.000, NL-3508 TA Utrecht, The Netherlands

Abstract. The reaction ^{2}H(e, $e'p$) has been studied at an invariant mass W of 1050 MeV, i.e. well below the $\Delta(1232)$ resonance. Cross sections have been obtained at values of Q^2, the four-momentum transfer squared, of 0.10, 0.20, and 0.28 (GeV/c)^2, covering a missing-momentum range from 150 to 700 MeV/c. The data are compared to the results of covariant calculations of Tjon, and the results of calculations based on a Schrödinger formalism due to Laget and the Mainz group, respectively. The data are well described by the calculations of the Mainz group, whereas they are underestimated by Tjon's calculations at high missing momenta. The calculations of Laget, on the other hand, overestimate the data at low missing momenta, but give a good account of the data at high missing momenta. More detailed considerations reveal that the $\Delta(1232)$ contributions are dominant at high missing momenta. However, the lacking $\Delta(1232)$ contribution in Tjon's calculations is not enough to explain the large discrepancy between his calculation and the present ^{2}H(e, $e'p$) data at high missing momentum. Probably the deuteron wave function employed in the covariant calculations has a D-state contribution that is too small.

1 Introduction

The deuteron wave function plays an important role in the description of many processes in subatomic physics. These include reactions such as elastic [1] and inelastic

* Dedicated to Prof. John A. Tjon on the occasion of his 60th birthday

electron scattering off the deuteron, and experiments aimed at extracting the electric form factor of the neutron G_E^n from quasi-elastic neutron knockout experiments on the deuteron [2]. Experimental information on the deuteron wave function can be obtained among others from deuteron electrodisintegration data. However, theoretical calculations for this ^{2}H(e, $e'p$) reaction show that the response functions not only depend on the details of the wave function, but also on contributions from meson-exchange currents (MEC), final-state interactions (FSI) and isobar currents (IC). Moreover, depending on the kinematic conditions, the coupling of the virtual photon to the neutron may become increasingly important. Hence, experiments aimed at obtaining information about the deuteron wave function need to be accompanied by detailed studies of the various interaction effects that also contribute to the ^{2}H(e, $e'p$) cross section.

Existing deuteron electrodisintegration experiments [3–6], which have provided cross-section data up to 300 MeV/c, are in general well described by the calculations. In this domain the interaction effects are relatively small, and the wave function is dominated by the S-wave component. Beyond 300 MeV/c few data are available. Bernheim et al. [3] have investigated the missing-momentum range 0–340 MeV/c in quasi-elastic kinematics. In other experiments, such as those described in ref. [7] (300–500 MeV/c) and ref. [8] (570–670 MeV/c), the measured cross sections were found to be dominated by IC, and revealed only little sensitivity to the deuteron wave function. At these large momenta the deuteron wave function is expected to be dominated by the D-state, whereas the contribution of the S-state is very small. Covariant calculations even predict effects from P-state components beyond 700 MeV/c [9, 10].

With the availability of the new generation of high-duty-factor electron accelerators (AmPS, MAMI, TJNAF), it is possible to study the high-momentum response of the ^{2}H(e, $e'p$) reaction in much more detail. Such data will provide constraints on the description of the various interaction effects that contribute to the ^{2}H(e, $e'p$) cross section in this domain, and are a prerequisite for more involved deuteron electrodisintegration studies aimed at determining the high-momentum part of the deuteron wave function itself.

In this paper such new ^{2}H($e, e'p$) data are presented. The experiments cover the missing-momentum range 150–700 MeV/c, for three values of the transferred four-momentum, i.e. Q^2 = 0.1, 0.2, and 0.3 (GeV/c)^2. In all cases the kinematics are centered at an invariant mass W = 1050 MeV. Given the experimental constraints on the beam energy (E_0 < 650 MeV) and the outgoing proton energy (T_p > 40 MeV), it was not possible to choose a lower value of W, while simultaneously requiring that enough energy is transferred to the deuteron to reach large nucleon momenta. Consequently, the invariant mass is somewhat closer to the Δ-region (W = 1232 MeV) than preferable for a pure quasi-elastic (e, $e'p$) experiment. Nevertheless, the measurements serve as an important benchmark for models describing the deuteron electrodisintegration process at high missing momentum, especially because the cross section was also measured as a function of the four-momentum transfer squared Q^2.

The experimental setup and the employed analysis techniques are briefly described in Sect. 2, which also includes an overview of the kinematical conditions. In Sect. 3 the data are presented in terms of a proton momentum distribution. The various calculations that are used for the interpretation of the data are briefly reviewed in Sect. 4. The comparison of these calculations to the experimental cross-section data is the subject of Sect. 5. In Sect. 6 we investigate the structure function R_T, which dominates the

cross section at large momenta, while the conclusions and an outlook are presented in Sect. 7.

2 Experimental Setup and Data Analysis

The experiment was carried out using the high-duty-factor electron beam from the Amsterdam Pulse Stretcher (AmPS). As a target a newly developed flowing liquid-deuterium system was employed, which is discussed in more detail in ref. [11]. One of the high-resolution spectrometers available in the EMIN hall at NIKHEF was used to detect the scattered electron. In conjunction with one of the spectrometers either the large solid-angle detector HADRON4 [13], or a second magnetic spectrometer was used for the detection of the ejected proton. The experimental setup is described in more detail in ref. [11].

The kinematic settings for the present experiments are summarized in Table 1. The data sets labelled L01–L03 were obtained with the QDQ and QDD spectrometers, and cover the low-missing-momentum domain. The data sets H01–H03 were obtained with the QDQ spectrometer and the HADRON4 scintillator detector. The large solid angle of HADRON4 (≈ 550 msr) makes it suitable to measure small cross sections, occurring in the reaction ^{2}H(e, $e'p$) at large missing momentum. The maximum luminosity to which HADRON4 can be exposed is limited by the single rates, since HADRON4 is a non-magnetic device. After optimising the duty factor and reducing the beam halo the maximum usable beam current was 2 μA for the present experiments (at a target thickness of 220 mg/cm^2), leading to a detector trigger dead-time of about 20%. As can be seen from Table 1, both the low- and high-missing-momentum regions have been studied at three values of the four-momentum transfer squared Q^2.

The analysis of the data involved several steps that differ somewhat depending on whether HADRON4 or the QDQ spectrometer was used for proton detection:

– The energy calibration of a spectrometer is obtained by means of (in)elastic electron scattering measurements at various incident energies [12]. For an open scintillator detector like HADRON4, the procedure is more involved as the response and offset of each of the 94 scintillator-photomultiplier combinations needs to be determined

Table 1. Kinematic variables for the ^{2}H(e, $e'p$) measurements presented in this paper. All data have been collected at an invariant mass of $W = 1050$ MeV. The electron kinematic variables Q^2, ω, and q are averaged over the full spectrometer acceptance. The ranges in p_m and in the angle γ_{pq} between the ejected proton and $\vec{q}$ result from the combined acceptances of the electron and proton detectors

Label	E_0 MeV	q MeV/c	ω MeV	Q^2 (GeV/c)^2	p_m MeV/c	γ_{pq} degr.
L01	603.8	359	170	0.10	225–315	26.5–37.9
L02	603.8	500	218	0.20	155–225	9.4–14.9
L03	603.8	615	275	0.30	150–310	10.2–26.5
H01	524.9	357	172	0.10	300–485	36.8–91.9
H02	575.9	498	224	0.20	320–595	33.0–92.1
H03	575.9	592	267	0.28	420–695	41.3–102.0

separately for each setting. This has been achieved by making use of $\Delta E - E$ correlation plots of two scintillators in consecutive layers.
- The calibration of the relative timing between the two detectors is described for the two-spectrometer case in ref. [12]. For measurements with HADRON4, the proton timing signal needs to be corrected for: (i) phase differences between individual counters; (ii) walk effects; (iii) light propagation time differences; and (iv) time-of-flight. Taking all these effects into account, a timing resolution of 0.75 ns (FWHM) was obtained [11].
- The efficiency of the detector systems was corrected for dead-time effects, multiple scattering, hadronic interactions and discriminator threshold effects. Moreover, as multiple hits cannot be properly handled by the data-acquisition system, they were rejected and – later-on – corrected for. This is of particular relevance for the HADRON4 data.
- The actual data were obtained by identifying the coincident $e - p$ events, subtracting accidental coincident events, correcting for acceptance effects and applying radiative corrections. Empty-target data were used to correct for events originating from the target cell walls. The timing differences between $\pi^- - p$ and $e - p$ events in combination with the response of an aerogel Cherenkov counter in the QDQ spectrometer allowed a very clean separation of $(e, e'p)$ and $(e, \pi^- p)$ events [14].

More details on the data analysis can be found in ref. [11], where it is also explained that the total systematic error in measurements L01 to L03 is about 6%, with a dominant contribution from the target thickness (3%). The measurements involving HADRON4 have a somewhat larger systematic uncertainty (8%) due to additional errors related to the alignment (4%), trigger efficiency (3%), and acceptance corrections (3%). Ref. [11] also contains a complete listing of the values of the measured cross sections.

3 The Proton Momentum Distribution

The results of the ^{2}H$(e, e'p)$ measurements are discussed in two representations. In this section the data are represented in terms of the proton momentum distribution, while cross sections are presented in Sect. 5.

In the plane-wave impulse approximation (PWIA) the incoming and scattered electron are described by plane waves, and the outgoing proton is assumed to have no interaction with the residual neutron. Moreover, it is also assumed that the properties of the proton in the deuteron are the same as for a free proton, and that the virtual photon couples to the proton that was actually detected. The combination of these assumptions leads to a factorized description of the $(e, e'p)$ cross section [15],

$$\frac{d^6\sigma}{d\epsilon'\, d\Omega_{\epsilon'}\, dT_p\, d\Omega_p} = pE_p\sigma_{ep}S(E_m, p_m), \tag{1}$$

where $p = |\vec{p}|$ and E_p are the three-momentum and energy of the ejected proton, and σ_{ep} is the (off-shell) electron-proton cross section for which – as usual – the current-conserving prescription by de Forest [16], i.e. σ_{ep}^{cc}, is taken. The spectral function $S(E_m, p_m)$ represents the probability to find a proton with a separation energy E_m and an initial momentum p_m in a nucleus. For the deuteron, E_m is equal to its binding energy of 2.225 MeV.

It is possible to evaluate a reduced cross section, or momentum distribution, obtained by integrating the cross section over the missing-energy range corresponding to one transition after dividing it by the factor $pE_p\sigma_{ep}$:

$$\rho(p_m) = \int_{\Delta E_m} \frac{d^6\sigma}{d\epsilon'\ d\Omega_{\epsilon'}\ dT_p\ d\Omega_p} \frac{1}{pE_p\sigma_{ep}} dE_m. \tag{2}$$

In PWIA, i.e. by neglecting FSI, MEC, and IC effect, the quantity $\rho(p_m)$ represents the proton wave function in momentum space. For the deuteron $\rho(p_m)$ can be rewritten as $u^2(p_m) + v^2(p_m)$, with u and v the S and D components of the wave function, respectively[1].

For the present experiment an invariant mass W = 1050 MeV was chosen, whereas $W = m_p = 938$ MeV corresponds to pure quasi-elastic kinematics. Moreover, at large values of p_m processes such as FSI or IC, which are otherwise small, are relatively more important. Hence, significant contributions from reaction-mechanism effects beyond PWIA are to be expected. Even so, it is useful to inspect the data in terms of $\rho(p_m)$ since the dependence on the basic electron kinematics is factored out. It also allows for an assessment of the global features of the data, especially concerning the basic processes driving the ^{2}H(e, $e'p$) response functions.

The upper panel of Fig. 1 shows the momentum distribution for all data sets listed in Table 1. Data sets obtained at the same value of Q^2 are represented by the same symbol. The data show the same behaviour irrespective of the value of Q^2, and are generally in agreement with each other to within 30%. Hence, the dependence of the cross section on Q^2 and E_0 is basically contained in σ_{ep}, indicating that the initial coupling involves a single nucleon, also at large values of p_m. Only the Q^2 = 0.2 (GeV/c)^2 data below p_m = 200 MeV/c seem to deviate from the global trend of the data. The kinematics for these data[2] were chosen such as to emphasize the contribution from the structure function R_{LT}. As the PWIA formalism is not suitable to accommodate differences in individual structure functions, this data set has been disregarded in the further analysis of the momentum distribution.

The remaining data sets were averaged per p_m bin. The result is shown in the lower panel of Fig. 1, together with the data obtained at Saclay [3]. In the region of overlap (150–350 MeV/c) the data sets are consistent up to 300 MeV/c. Beyond this point the two data sets diverge, what might be related to the lower value of W employed at Saclay ($W \approx$ 950 MeV), as will be discussed in Sect. 5. The present data decrease steeply until p_m = 300 MeV/c, but the data are roughly constant at larger values of p_m. Compared to the momentum distribution derived from the Bonn potential [20], the discrepancy at high p_m is large, suggesting that other reaction processes rather than an anomalous behaviour of the deuteron wave function are at the origin of this effect. The comparison to the Bonn calculation also shows that beyond 350 MeV/c the PWIA cross section is largely determined by the D-state component of the deuteron wave function.

[1] The small P-wave amplitudes predicted by covariant formalisms are not considered in this discussion

[2] This data set was also used in ref. [17] to demonstrate that R_{LT} is in fact rather large. A state-of-the-art ^{2}H(e, $e'p$) model can properly account for these data [17]

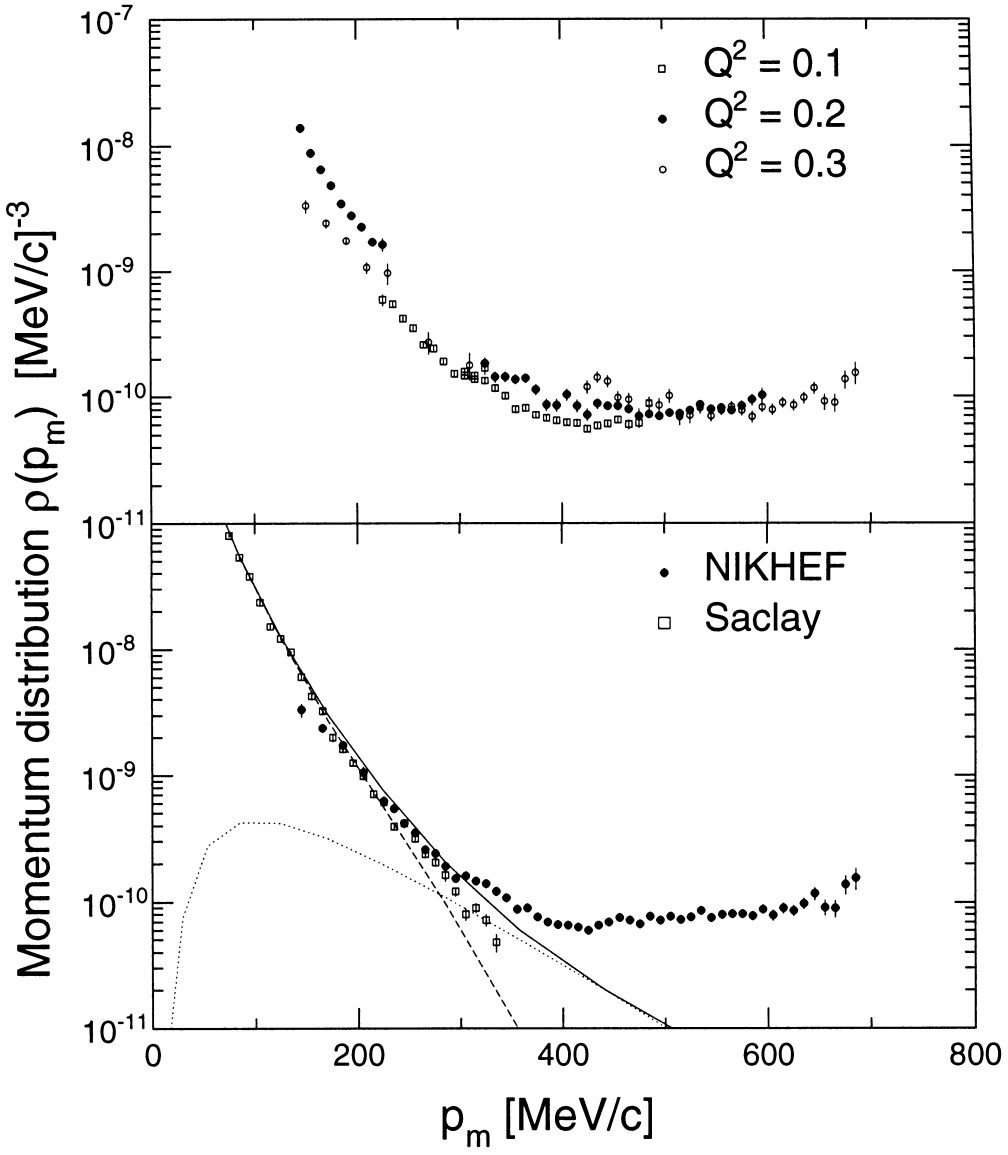

Fig. 1. The upper panel shows the ^{2}H(e, $e'p$) momentum distributions evaluated from the present data. The transferred four-momentum Q^2 is given in units of (GeV/c)^2. The lower panel shows the average of the data not including the $Q^2 = 0.2$ (GeV/c)^2 data below $p_m = 200$ MeV/c. Also shown are the Saclay data (open squares). The full curve is the deuteron momentum distribution derived from the Bonn potential, the dashed curve representing the *S*-wave contribution, the dotted one the *D*-wave contribution

4 Theoretical Description

The cross-section data are compared to the results of various calculations in Sect. 5. In this section the ingredients of the three theoretical frameworks that have been used for the interpretation of the data are discussed. These concern the models of the Mainz group, of Laget, and of Tjon, respectively. Calculations by Mosconi [18, 19] are also available, but these are restricted to small values of q. For that reason

they are not included in the current section, but are presented separately in the Appendix.

All calculations are available with different aspects of the reaction mechanism switched on or off. In the PWIA calculations the virtual photon couples only to the proton, and FSI are not included. In the plane-wave Born approximation (PWBA) the photon may in addition couple to the neutron, and when FSI are added the full calculation is obtained. Finally, the effects of IC may be taken into account.

The calculations of the Mainz group [21, 22], are performed in a nonrelativistic framework. The interaction used to calculate the deuteron wave function is a realistic nucleon-nucleon (*NN*) potential. For the current calculations in particular the Bonn [20] potential was employed. The usual terms describing the coupling of the virtual photon to the proton and the neutron (Born term) are at the basis of the calculation. In the full calculation all leading order π- and ρ-meson-exchange contributions are included, as well as the static heavy-meson-exchange contributions from δ, η, σ, and ω. These contributions are also included in the *NN* interaction. In addition, $\gamma\pi\rho$ and $\gamma\pi\omega$ couplings are taken into account. The full calculations also include FSI for partial waves up to $j = 5$. A dynamical treatment of the Δ contribution is realized through a *NN*-*N*Δ coupled-channels (CC) approach. This introduces Δ-isobar degrees of freedom into the wave function. Furthermore, π- and ρ-exchange currents related to these transitions are included. Relativistic corrections for most elements of the current operator, including those for MEC, but not for IC, are incorporated through a p/M expansion in a self-consistent way [22].

Laget uses an approach in which he includes explicit diagrams for the various reaction processes [23, 24]. The wave function is constructed using the Paris potential [25]. FSI are included, but limited to *S*, *P*, and *D*-waves, i.e. $j \leqslant 2$. MEC are included through π and ρ exchange. The Δ-isobar is accounted for through the diagram in which the Δ is excited by the interaction with the virtual photon, and subsequently decays by one-pion exchange. Relativistic corrections are applied up to order $(p/M)^3$. Laget's calculations are limited to one-loop dominant diagrams.

The formalism used by Tjon is described in ref. [26]. He uses a Lorenz-covariant approach, in contrast to Laget and the Mainz group, who use a nonrelativistic approach. The calculations are performed within a Bethe-Salpeter framework using a quasi-potential approximation, where the two-particle propagator is replaced by one where the relative nucleon energy is constrained. The quasi-potential approximation by Blankenbecler, Sugar, Logunov, and Tavkhelidze (BSLT) was applied. Using this approach a consistent treatment of the electromagnetic current and the *NN* interaction is realized through a one-boson-exchange model, including MEC contributions and FSI. The FSI are calculated up to $j = 9$. The negative energy states, which occur in covariant calculations, are usually small and neglected in the current work. Isobar contributions are not taken into account, contrary to the calculations of Laget and the Mainz group.

5 Cross-Section Results

Fig. 2 shows the cross sections evaluated for the data sets L01, L02, and L03. The solid curves represent the full calculations of the Mainz group [21], the dashed curves are due to Laget [27], and the dotted to Tjon [28]. The calculations of the Mainz group and of Laget have not been corrected for acceptance effects of the experimental setup [11]. The

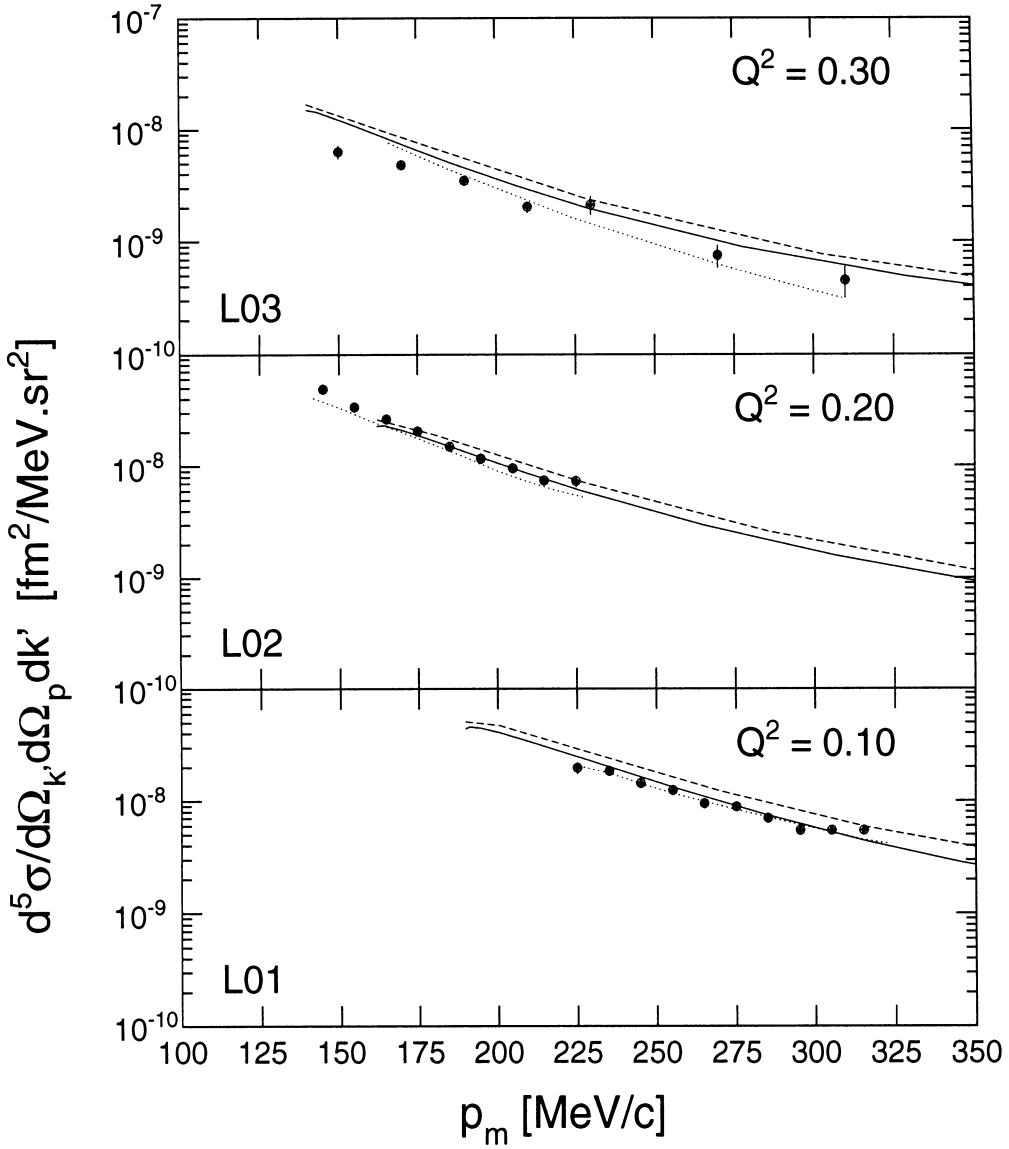

Fig. 2. Cross-section data for the reaction ^{2}H(e, $e'p$) at $E_0 = 604$ MeV and W = 1050 MeV. The solid curves represent the calculations of the Mainz group, the dotted those of Tjon, and the dashed those of Laget. The nonrelativistic calculations of the Mainz group and of Laget include FSI, Δ, MEC contributions and relativistic corrections. The covariant calculations of Tjon include FSI and MEC contributions only

influence of these effects on the cross section is less than 3% except for the two lowest and highest p_m-points for each data set, where it is at most 10%. The most prominent effect shows up in data set L02, where the experimental acceptance gives access to lower missing momenta than would have been possible if only the central electron kinematics were considered. The calculations of the Mainz group and of Laget are evaluated for the central kinematics. At missing momentum values of 280 MeV/c (L01), 195 MeV/c (L02), 190 and 290 MeV/c (L03) the kinematics used in the calculations match those of the data exactly.

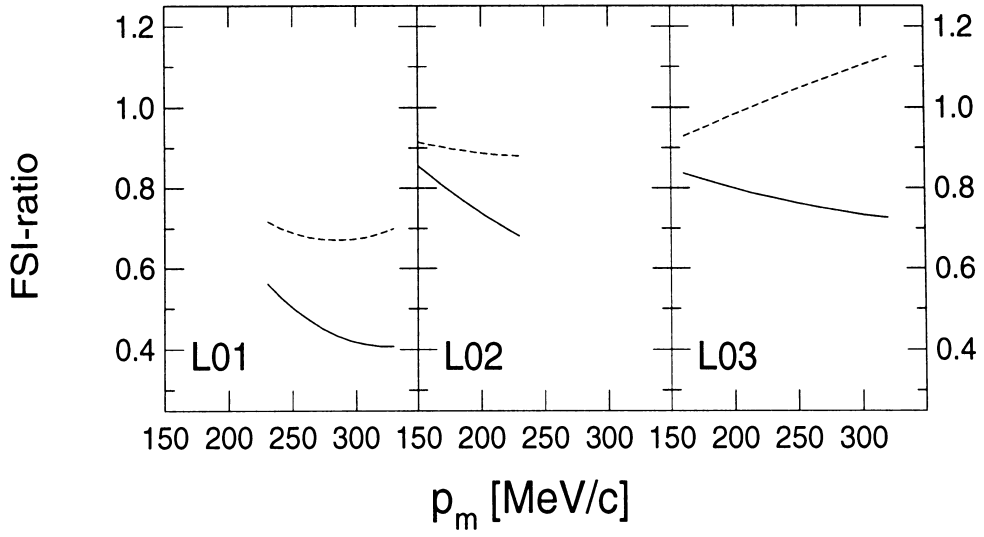

Fig. 3. Ratio of PWBA + FSI and PWBA calculations of the Mainz group (solid curve) and of Laget (dashed curve), for the data sets L01–L03

The calculations both of Tjon and the Mainz group give a good account of the data for the three values of Q^2. The results of Laget's calculations are also close to the data, but generally overestimate the cross section. Especially for the data set L01 a systematic discrepancy with the data of approximately 20% is observed. Since Laget's model is more similar to that of the Mainz group than to Tjon's, the Laget and Mainz models are compared in Fig. 3, where the ratios of the PWBA + FSI to PWBA calculations are shown. The PWBA calculations contain the PWIA diagram and the Born term, but no MEC, FSI or IC. The FSI calculations have the same ingredients as the PWBA calculations, with rescattering contributions added. The three panels show that the Mainz group attributes a stronger effect to the FSI than Laget does, i.e. leading to smaller values of the ratio displayed in Fig. 3. This suggests that Laget's calculation underestimates the FSI, what is possibly caused by the limited number of partial waves taken into account. The general overestimate of the data can be explained in this way. A similar result was reported in ref. [23].

Fig. 4 shows the high-missing-momenta data sets H01–H03, which employed the HADRON4 detector for proton detection. The acceptance effects for these kinematics are minimal, because the large acceptance of HADRON4 ensures that for almost all p_m values the entire electron-spectrometer acceptance is used. The measured cross section is an average over many (q, ω) values, since these differ for each event. The averaging procedure is only valid if the cross section is a linear function of q and ω. The linearity was verified using calculations by Tjon and found to be valid within 3%, which is well within the systematic uncertainty of the present data.

The large solid angle of HADRON4 introduces a minor complication when comparing the data with calculations, since the out-of-plane acceptance of this detector is sizeable, i.e. $\pm 22°$. The calculations have not been evaluated at the average out-of-plane angle ϕ_{opl}, but assume that $\phi_{\mathrm{opl}} = \pi$ instead. The combined contribution of the structure functions R_{LT} and R_{TT}, which depend on ϕ_{opl}, is always less than 20%

according to the Mainz calculations [8, 21, 22]. As the average over a p_m-bin of $\cos\phi_{\rm opl}$ and $\cos 2\phi_{\rm opl}$ amounts to ≈ 0.97 and ≈ 0.87 for most p_m-bins, the average effect consists of a global decrease of the calculated values by approximately 2%, depending on the relative contribution of R_{LT} and R_{TT}. For the lowest p_m-values the effect is slightly larger, i.e. $\approx 5\%$. As the effect is well within the systematic error on the data of 8%, no corrections have been applied.

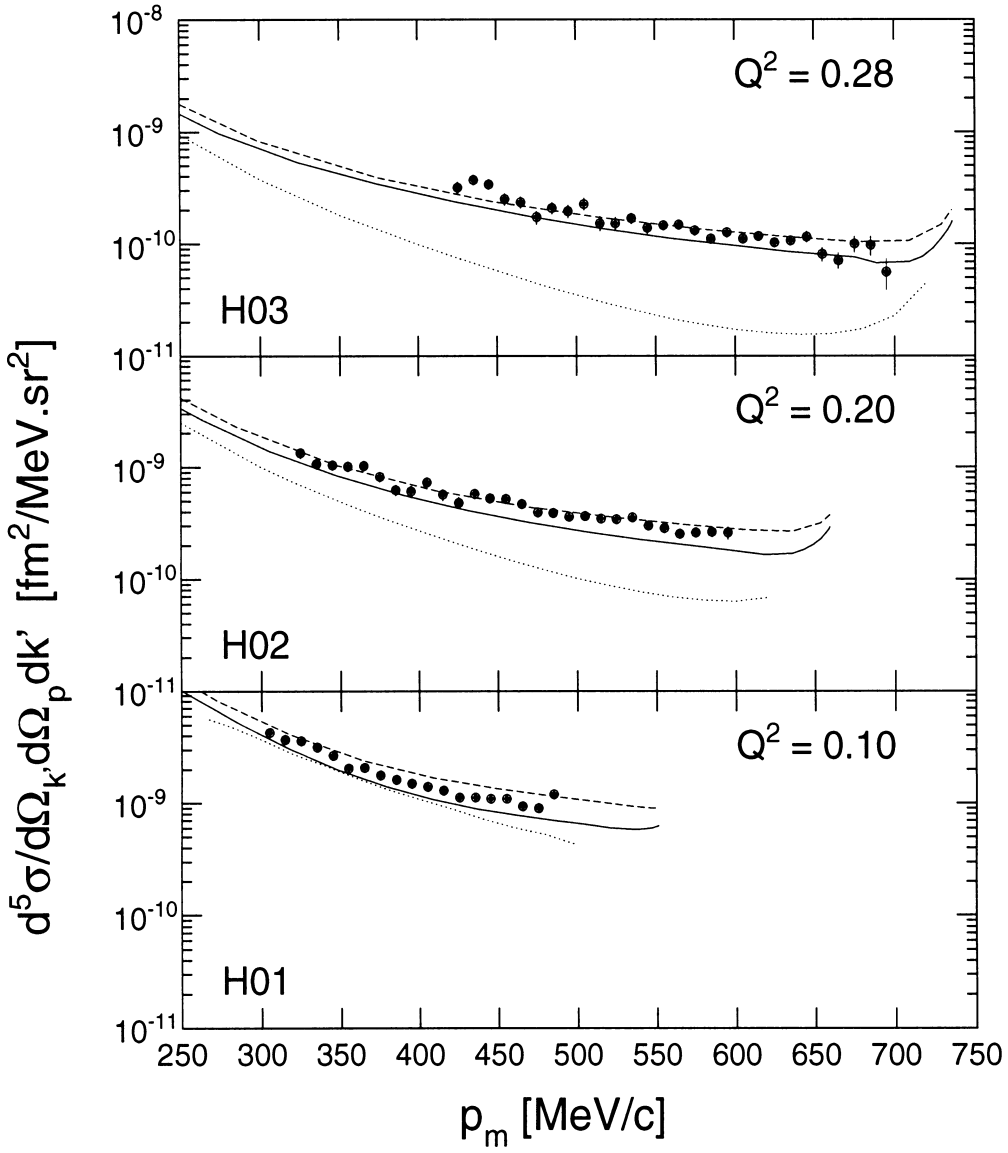

Fig. 4. Cross-section data for the reaction ^{2}H(e, $e'p$) at $E_0 = 525$ MeV (lower panel) and $E_0 = 576$ MeV (upper two panels), and $W = 1050$ MeV. The solid curves represent calculations of the Mainz group, the dashed curves those of Laget, the dotted those of Tjon. The upswing of the calculations at the highest p_m values is caused by the direct coupling of the photon to the neutron (Born term)

Laget's calculations are quite successful in describing the high-p_m data sets. At $Q^2 = 0.20$ (GeV/c)^2 and 0.28 (GeV/c)^2 his calculations are in complete agreement with the data, but at Q^2 = 0.10 (GeV/c)^2 the calculations overestimate the data by almost 20%. When these findings are compared with Laget's overestimate of the L01 data, it is concluded that the accuracy of his description depends on Q^2. This suggests that one of the reaction processes is not well accounted for. In view of the comparison displayed in Fig. 3, this is likely to be the incomplete description of FSI effects.

The full CC calculations of the Mainz group give a similarly good description of the data as Laget's calculations. On average the data are underestimated by typically 20%, but the trend of the data is well reproduced. This underestimate is not present at the low-p_m data sets L01–L03, and neither does it depend on Q^2 or p_m within these data sets. Calculations with and without relativistic corrections are available. The latter ones are not shown in the figures. The effect of incorporating relativistic effects in the calculations varies from a 2% reduction at low p_m to a 15% reduction at high p_m.

Fig. 5 shows the relative contribution of the Δ resonance to the cross section for the Mainz and Laget calculations. The two models agree reasonably well on the magnitude of the Δ contributions, although the Mainz calculation is systematically larger.

At high p_m (γ_{pq}) the Δ contribution is much stronger than at low p_m. Since the Mainz calculations describe the low-p_m data quite well, the remaining discrepancy with the high-p_m data might be caused by an underestimate of the Δ contribution.

Tjon's calculations show a remarkable deviation from the data at increasing values of Q^2. At $Q^2 = 0.10$ (GeV/c)^2 the deviation is least, but still ranges from 20% at $p_m = 300$ MeV/c to 50% at $p_m = 470$ MeV/c. At $Q^2 = 0.28$ (GeV/c)^2 the discrepancy increases to more than one order of magnitude. Tjon's calculations differ from those of

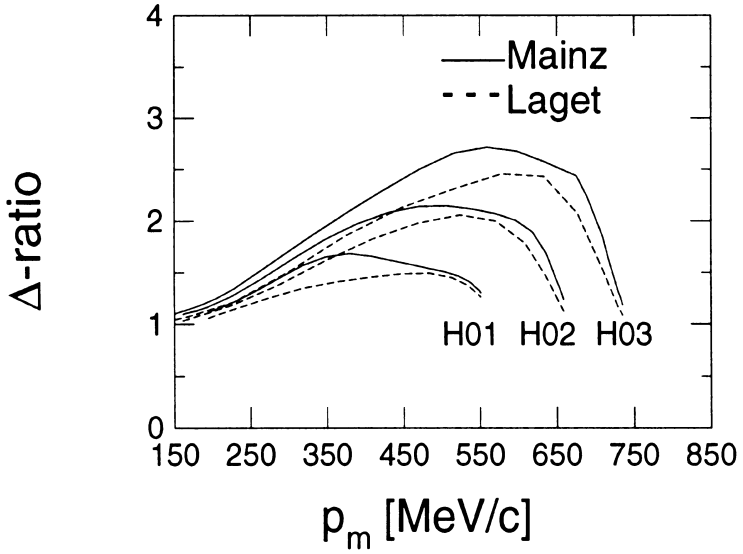

Fig. 5. The ratio of full calculations to those without the Δ contribution, for the Mainz model (solid curve) and Laget's model (dashed curve) in the kinematics of data sets H01–H03. The ratios belonging to the L01–L03 data sets (not shown) are very similar

Laget and the Mainz group in a number of ways. One of the most important differences is that he does not take into account IC. Furthermore, where the Mainz group and Laget include relativistic corrections to the current operator, Tjon's calculations are covariant, although in the present Q^2 domain this is not expected to be a dominant effect (see ref. [17]). He employs a *NN* potential based on the BSLT approximation [26], instead of the Paris (Laget) or Bonn (Mainz group) potentials. Finally, in the current calculations

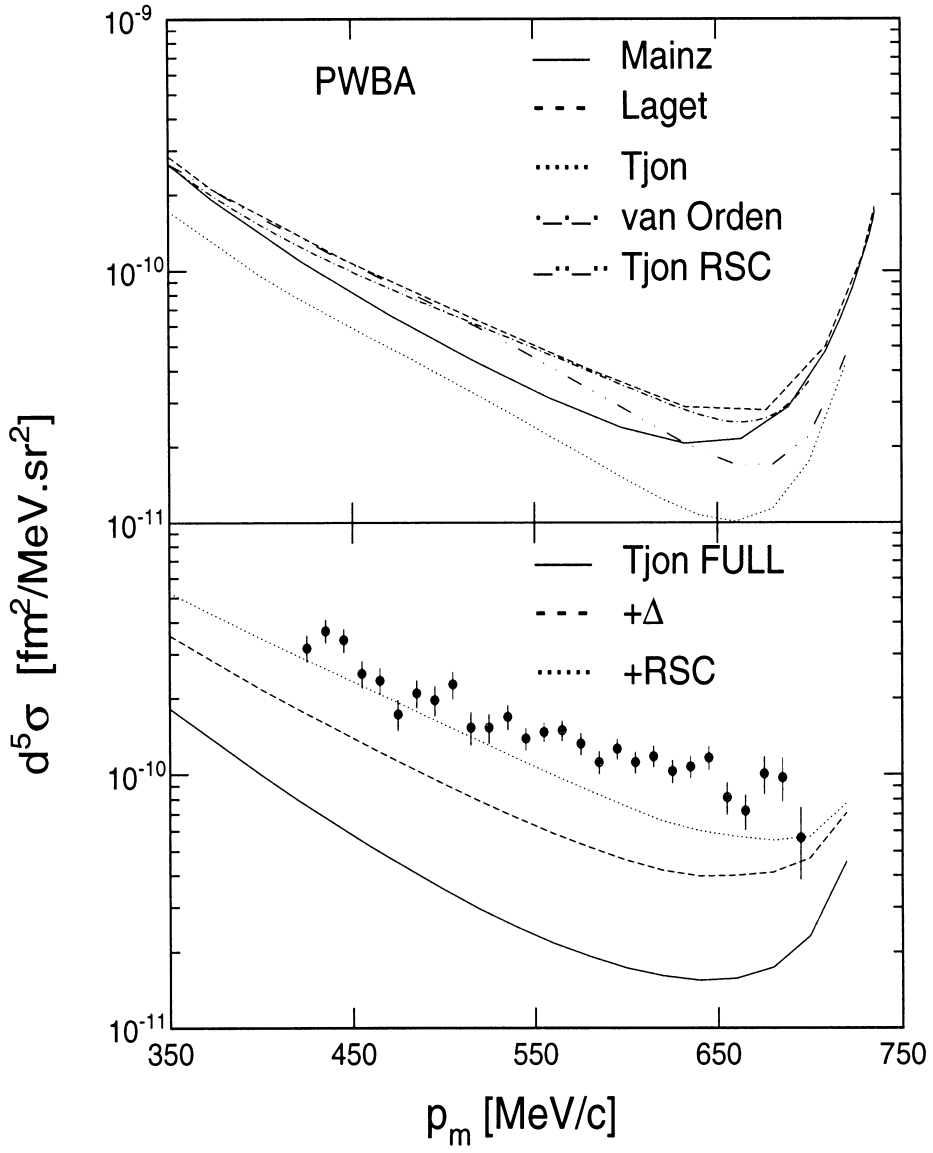

Fig. 6. The upper panel shows PWBA calculations of the Mainz group, Laget, Tjon (BSLT and RSC potential), and van Orden. The lower panel shows three calculations by Tjon: the full calculation (solid curve), the dashed curve (+Δ) represents the same calculation multiplied by an estimate of the Δ contribution derived from the Mainz calculation (Fig. 5), and the dotted curve is the result of replacing the BSLT-based *NN*-potential by the RSC potential, in addition to the Δ correction. The data shown are from set H03

negative-energy states are not taken into account, since these are expected to be small and are very time consuming to calculate. Some trial calculations indicated an increase of the cross section due to the inclusion of negative-energy states by at most 10%, as evaluated for data set H03 at $p_m = 640\,\mathrm{MeV}/c$ [28].

In order to investigate the origin of this discrepancy in more detail the upper panel of Fig. 6 shows PWBA calculations as obtained from the various authors. Included are processes where the virtual photon couples to the proton or neutron and MEC currents, but no FSI or IC, are incorporated. Apart from the calculations of the Mainz group, Laget and Tjon, results are shown from a covariant calculation performed by van Orden and Gross [29]. In this approach the authors use the same Bethe-Salpeter framework for deuteron electrodisintegration as is used by Tjon. Instead of the BSLT approximation for the evaluation of the wave function and propagator, however, the spectator — or Gross — equation is used. In this approximation one of the nucleons (the spectator) is restricted to its mass shell. The *NN* interaction is constructed using the Gross equation. Since their $(e, e'p)$ calculations are under development, no FSI or IC effects can currently be computed. A full reference is not yet available, but some details are given in [10] and [30].

Van Orden's PWBA calculation is very close to Laget's, who employs the Paris potential. The calculations of the Mainz group are somewhat lower, but the original calculation by Tjon is clearly well below the other calculations. However, if the BSLT deuteron vertex function is replaced by the Reid soft-core (RSC) vertex function, the resulting curve (double-dot-dashed) is compatible with the other PWBA calculations. It is concluded that the BSLT wave function is not consistent with other deuteron wave functions at these high momenta.

The full curve in the lower panel of Fig. 6 shows the original calculation from Tjon, including FSI effects. This calculation naturally underestimates the data, since the Δ contribution is not taken into account. In order to estimate the effect of the isobar currents, Tjon's full calculation is multiplied by the Mainz Δ ratio, resulting in the dashed curve shown in the lower panel. Although this curve is now much closer to the data, it is still significantly below them. If in addition the BSLT *NN* potential is replaced by the RSC potential, the resulting dotted curve is in fair agreement with the data. In fact, this is as good a description of the data as the Mainz calculation of Fig. 4, upper panel. Since the RSC wave function has a larger *D*-state probability (6.7%) than the BSLT one (4.7%), the difference between the BSLT-based cross section and the ones obtained with the RSC wave function might be related to the size of the *D*-state component. Inspection of Fig. 1 indeed shows that in the p_m-range from 300 to 500 MeV/*c* the cross section is dominated by the *D*-state component. However, at present the data cannot (yet) be used to constrain the size of the *D*-state component. This is illustrated by the different values of the *D*-state probability used by the Mainz group (4.2%) and Laget (5.8%), which both give a fairly good description of the data.

6 The R_T Structure Function

It is of interest to compare the predictions of the various models for individual structure functions. In particular, Fig. 7 shows the contribution of the transverse structure function R_T to the five-fold differential cross section. By comparing to the top panel

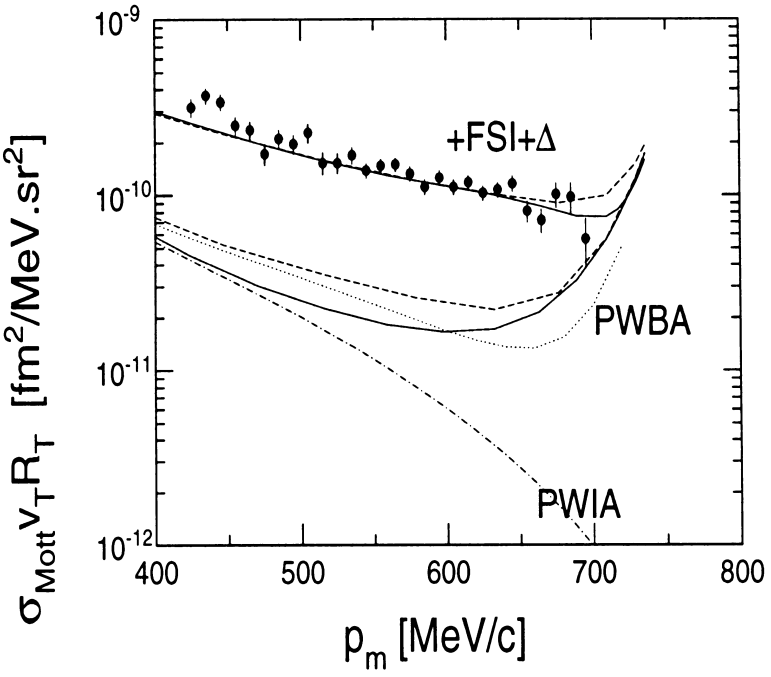

Fig. 7. The contribution of structure function R_T to the cross section. The solid curves are due to the Mainz group and the dashed curves due to Laget. The upper two curves, which are labelled by $+\text{FSI} + \Delta$, represent the full calculations. The middle two curves are PWBA calculations without FSI or Δ. The dotted and dot-dashed curves represent PWBA and PWIA calculations by Tjon in which the RSC potential was employed. The data are from set H03 at $Q^2 = 0.28$ (GeV/c)^2

of Fig. 4, it is concluded that for both the Mainz and Laget calculations the cross section is dominated by R_T. Their PWBA calculations show that the relatively large size of R_T is driven by the Δ contribution. This is to be expected because of dominance of the transverse $M1$ transition, which determines approximately 99% of the response [31].

The upswing of the curves at the highest values of p_m has a common origin, as is illustrated by Tjon's calculations in Fig. 7. The PWIA calculation (dot-dashed) contains only a term in which the virtual photon couples to the proton, while the PWBA calculation (dotted) also includes the coupling to the neutron, which is transverse as the neutron has no charge.

If the models are correct in attributing more than 90% of the total response to R_T, this structure function may be directly evaluated from the measured cross section under the given kinematic conditions, i.e. at large proton angles where the Δ resonance is found to be dominant.

7 Conclusions and Outlook

The reaction ^{2}H(e, $e'p$) has been studied at large missing momenta (150–700 MeV/c) for three values of Q^2. A proton momentum distribution has been derived from the data, which is well described up to $p_m = 300$ MeV/c. At larger momenta a sizeable discrepancy between the PWIA curves and the data develops. From the comparison

between the cross-section data and various calculations it is learned that at large missing momenta the Δ isobar is of increasing importance. At the chosen value of the invariant mass (W = 1050 MeV) the Δ resonance is already seen to dominate the high-missing-momentum part of the cross section.

The Mainz group offers the best global description of the cross-section data. The low-p_m data are well described within the experimental errors, and the high-p_m data are underestimated only by approximately 20%.

The approach of Laget does very well for the high-p_m data sets H01–H03, but a clear overestimate at low p_m was observed. By comparing the calculations to those of the Mainz group, the discrepancy has been attributed to an incomplete treatment of FSI effects. At high p_m the underestimate of the FSI is partly compensated by an underestimate of IC effects.

The present covariant calculations by Tjon do not include IC contributions, and hence cannot describe the data beyond $p_m = 300\,\mathrm{MeV}/c$. In addition, when compared to other calculations and the data, Tjon's calculations show that the current BSLT wave function may not be correct at large momenta. If the BSLT-based *NN* interaction is replaced by the RSC potential, Tjon's calculation is enhanced by as much as 60%. This result suggests a potential sensitivity of the present data to the size of the *D*-state component in the deuteron wave function.

In summary, the mechanism of deuteron electrodisintegration has been studied for the first time in the high-missing-momentum domain. Current state-of-the-art calculations are more or less able to describe the data. In order to exploit the potential sensitivity of the cross section to the *D*-state component of the deuteron wave function, measurements at $W \approx 950\,\mathrm{MeV}$ are needed that – preferably – include a separation of the longitudinal and transverse response functions.

Acknowledgement. This work is part of the research program of the FOM Institute for Subatomic Physics, NIKHEF, which is financially supported by the Netherlands' Organisation for Scientific Research (NWO).

Appendix A. Calculations by Mosconi

Four different calculations have been performed for the interpretation of the high-p_m ^{2}H(e, $e'p$) data presented in this paper. In the main text of the paper the discussion was restricted to three of these sets, i.e. the ones by Laget, Tjon, and the Mainz group, as these calculations represent different theoretical approaches to the treatment of deuterium electrodisintegration. The fourth calculation, carried out by Mosconi [18], is similar in approach to that of the Mainz group, and for that reason was not shown in the main body of the paper. However, for future reference it is useful to show also the comparison of the Mosconi calculation to the data. Moreover, the subtle differences between the Mosconi calculations and those of the Mainz group [21] can provide further information on the mechanism of the ^{2}H(e, $e'p$) reaction at high p_m. For these reasons a separate comparison of the Mosconi calculations to the data (and the Mainz calculations) is presented in this Appendix.

The Mosconi calculations [19] are based on the Schrödinger formalism. The effects of MEC and FSI are included, and IC are treated in a static approximation of the Δ propagator. Relativistic corrections are applied in the form of a q/M expansion of second order. The *NN* interaction used is based on the Paris potential. The key differences with the work of the Mainz group concern the treatment of the Δ resonance and the *NN* interaction employed. The Mainz group includes a more comprehensive treatment of the Δ by using a coupled channels approach (see Sect. 4). They employ a deuteron wave function derived from the

Bonn potential with a *D*-state probability of 4.2%, while the Paris potential leads to a 5.8% *D*-state probability.

Mosconi has performed calculations for the data sets labelled L01, L02, H01, and H02, whose kinematical settings are listed in Table 1. No calculations have been performed for the kinematical settings L03 and H03 since the (q, ω) of these settings are too high for the approximations made in this approach.

Fig. A.1 shows the data sets L01 and L02, covering the low-p_m domain, together with the predictions from the Mainz group [21] and those of Mosconi [18]. As opposed to the Mainz calculations, the Mosconi calculations include the effects of the detector acceptances [11]. His calculation for the L01 data set describes the data very well, whereas the same calculation for the L02 data slightly overestimates the data. The Mosconi results are very similar to those of the Mainz group, and it can be fairly stated that in this domain of p_m and Q^2 the two approaches are both in agreement with the data.

In Fig. A.2 Mosconi's calculations are compared to the high-p_m data sets H01 and H02. His calculations underestimate both data sets significantly. Whereas they follow the predictions of the Mainz group at lower p_m, an increasing discrepancy is observed at higher p_m. This discrepancy is likely to be due to one of the key differences with the Mainz calculations, i.e. the treatment of the IC contributions.

Fig. A.3 shows the relative contribution of the Δ resonance to the cross section. Remarkably, Mosconi predicts a much lower IC contribution, which is likely to be the cause of the observed underestimate of the data. The comparison of Mosconi's calculations to the high-p_m data demonstrates – once more – the sensitivity of high-p_m ^{2}H(e, $e'p$) data to a proper treatment of the IC contribution.

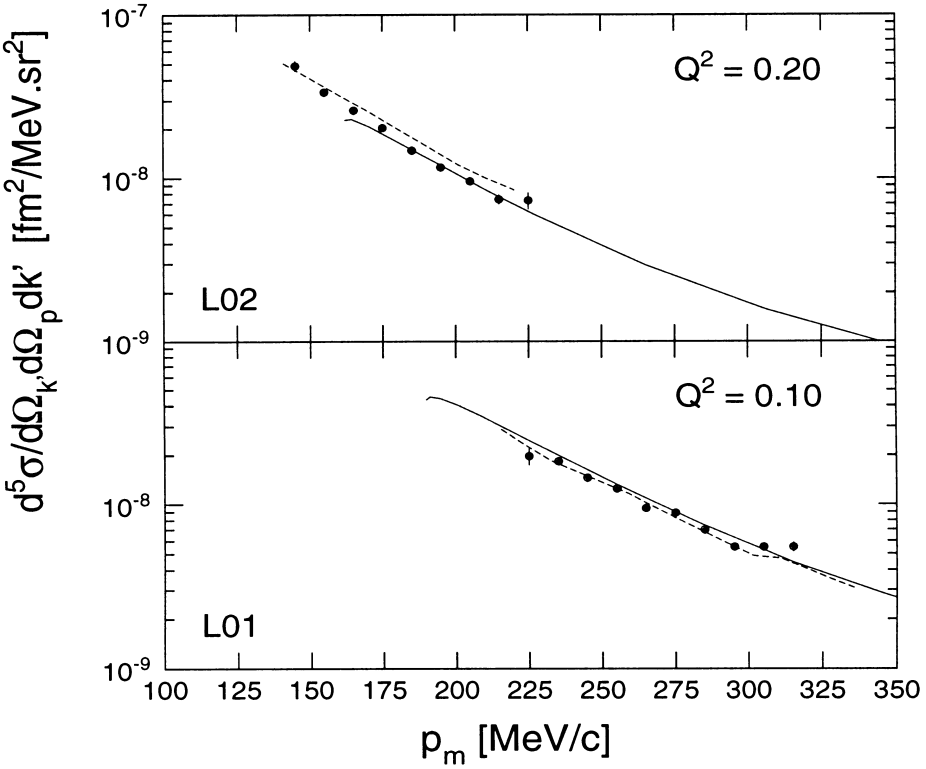

Fig. A.1. Cross-section data for the reaction ^{2}H(e, $e'p$) at $E_0 = 604$ MeV and $W = 1050$ MeV at two values of the four-momentum transfer Q^2 given in units of (GeV/c)^2. The solid curves represent calculations of the Mainz group, the dashed curves are calculations of Mosconi

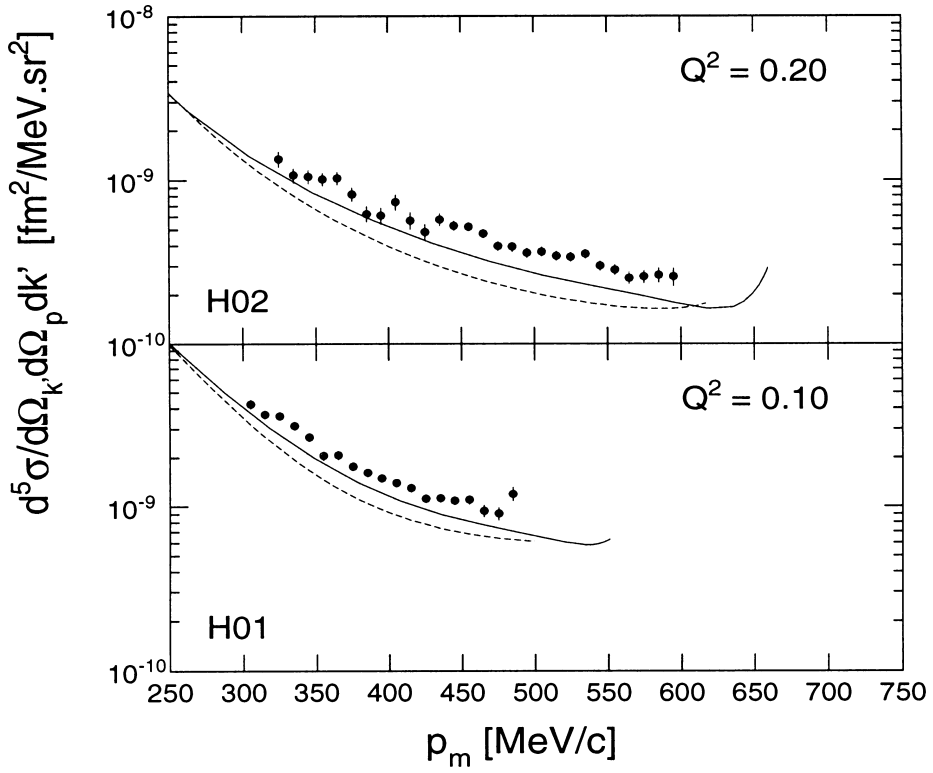

Fig. A.2. Cross-section data for the reaction ^{2}H(e, $e'p$) at Q^2 = 0.2 (GeV/c)^2 (upper panel) and $Q^2 = 0.1$ (GeV/c)^2 (lower panel), and $W = 1050$ MeV. The solid curves represent the Mainz calculations and the dashed curves those of Mosconi

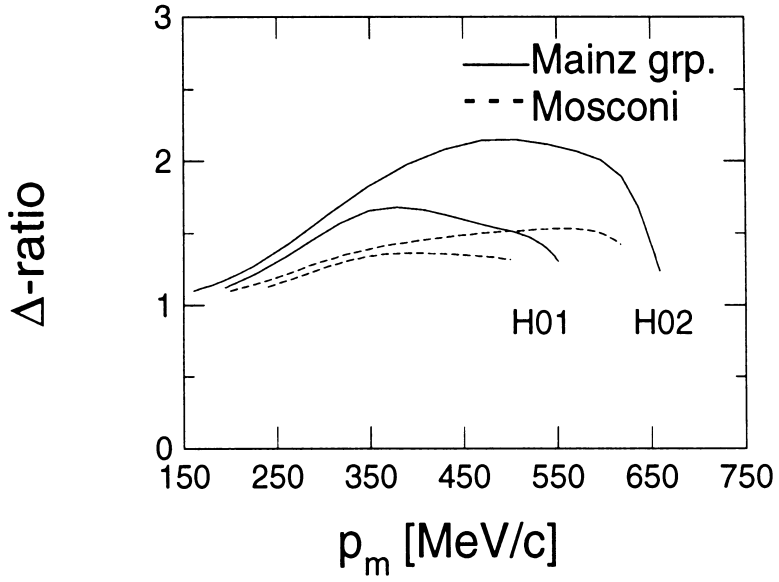

Fig. A.3. The ratio of full calculations to those without the Δ contribution, for the calculations of the Mainz group (solid curve) and of Mosconi (dashed curve) for the data sets H01–H02

Note Added in Proof

After the acceptance for publication of the present manuscript, the results of a similar ^{2}H$(e, e'p)$ experiment were published elsewhere (Blomqvist, K. I., et al.: Phys. Lett. **B424**, 33 (1998)), confirming the conclusions of the present experiment.

References

1. Lomon, E. L.: Ann. Phys. (NY) **125**, 309 (1980)
2. Kelly, J. J.: Adv. Nucl. Phys. **23**, 75 (1996)
3. Bernheim, M., et al.: Nucl. Phys. **A365**, 349 (1981)
4. Bulten, H. J., et al.: Phys. Rev. Lett. **74**, 4775 (1995)
5. Ducret, J. E., et al.: Phys. Rev. **C49**, 1783 (1994)
6. Van der Schaar, M., et al.: Phys. Rev. Lett. **68**, 776 (1992)
7. Turck-Chieze, S., et al.: Phys. Lett. **B142**, 145 (1984)
8. Pellegrino, A., et al.: Phys. Rev. Lett. **78**, 4011 (1997)
9. Buck, W. W., Gross, F.: Phys. Rev. **D20**, 2361 (1979)
10. Gross, F., Van Orden, J. W., Holinde, K.: Phys. Rev. **C45**, 2094 (1992)
11. Kasdorp, W.-J.: Ph.D. Thesis, Universiteit Utrecht 1997 (unpublished)
12. De Vries, C., et al.: Nucl. Instr. Meth. **A249**, 337 (1984)
13. Zondervan, A., et al.: Nucl. Instr. Meth. **A342**, 436 (1994)
14. Van der Steenhoven, G., et al.: Nucl. Instr. Meth. **A399**, 160 (1997)
15. Mougey, J., et al.: Nucl. Phys. **A262**, 461 (1976)
16. De Forest Jr., T.: Nucl. Phys. **A392**, 232 (1982)
17. Kasdorp, W.-J., et al.: Phys. Lett. **B393**, 42 (1997)
18. Mosconi, B.: Private communication (1996)
19. Mosconi, B., Pauschenwein, J., Ricci, P.: Phys. Rev. **C48**, 332 (1993)
20. Machleidt, R., Holinde, K., Elster, Ch.: Phys. Rep. **149**, 1 (1987)
21. Ritz, F., Leidemann, W.: Private communication (1997); Ritz, F., Göller, H., Wilbois, T., Arenhövel, H.: Phys. Rev. **C55**, 2214 (1997)
22. Beck, G., Arenhövel, H.: Few-Body Systems **13**, 165 (1992); **15**, 37 (1993); Wilbois, T., Beck, G., Arenhövel, H.: Few-Body Systems **15**, 39 (1993); Beck, G., Wilbois, T., Arenhövel, H.: Few-Body Systems **17**, 91 (1994)
23. Laget, J. M.: Can. J. Phys. **62**, 1046 (1984)
24. Laget, J. M.: Phys. Lett. **B199**, 493 (1987)
25. Lacombe, M., et al.: Phys. Rev. **C21**, 861 (1980)
26. Hummel, E., Tjon, J. A.: Phys. Rev. **C49**, 21 (1994)
27. Laget, J. M.: Private communication (1996)
28. Tjon, J. A.: Private communication (1996)
29. Van Orden, J. W.: Private communication (1996)
30. Van Orden, J. W., Devine, N., Gross, F.: Phys. Rev. Lett. **75**, 4369 (1995); Van Orden, J. W.: Czech. J. Phys. **45**, 181 (1995); Van Orden, J. W., Devine, N., Gross, F.: Few-Body Systems Suppl. **9**, 415 (1995)
31. Li, X., Wright, L. E., Bennhold, C.: Phys. Rev. **C48**, 816 (1993)

Received August 19, 1997; revised January 28, 1998; accepted for publication February 17, 1998